Noname manuscript No.
(will be inserted by the editor)

Modeling LSD1-Mediated Tumor Stagnation

Jesse Milzman · Wanqiang Sheng · Doron Levy

Received: date / Accepted: date

Abstract LSD1 (KDMA1) has gained attention in the last decade as a cancer biomarker and drug target. In particular, recent work suggests that LSD1 inhibition reduces tumor growth, increases T cell tumor infiltration, and complements PD1/PDL1 checkpoint inhibitor therapy. In order to elucidate the immunogenic effects of LSD1 inhibition, we develop a mathematical model of tumor growth under the influence of the adaptive immune response. In particular, we investigate the anti-tumor cytotoxicity of LSD1-mediated T cell dynamics, in order to better understand the synergistic potential of LSD1 inhibition in combination immunotherapies, including checkpoint inhibitors. To that end, we formulate a nonspatial delay differential equation model, and fit to the B16 mouse model data from Sheng *et al.*[*Cell.* 174, 3. (2018)]. Our results suggest that the immunogenic effect of LSD1 inhibition accelerates anti-tumor cytoxicity. However, cytotoxicity does not seem to account for the slower growth observed in LSD1 inhibited tumors, despite evidence suggesting immune-mediation of this effect.

J. Milzman
Department of Mathematics and Center for Scientific Computation and Mathematical Modeling (CSCAMM), University of Maryland, College Park, MD 20742, USA
E-mail: jmilzman@umd.edu

W. Sheng
Department of Cell Biology, Harvard Medical School and Division of Newborn Medicine and Epigenetics Program, Boston Children's Hospital, Boston, MA 02115, USA
E-mail: Wanqiang.Sheng@childrens.harvard.edu

D. Levy
Department of Mathematics and Center for Scientific Computation and Mathematical Modeling (CSCAMM), University of Maryland, College Park, MD 20742, USA
E-mail: dlevy@math.umd.edu

1 Introduction

The gene coding for the histone lysine-specific demethylase LSD1 (KDMA1) has gained attention in the last decade as a cancer cell biomarker. It has been shown to mediate disease progression in multiple cancers, including acute myeloid leukemia [15, 32, 37] as well as carcinomas of the breast [29, 39], liver [36], prostate, bladder, colon, and lung [16], among others. Thus, LSD1 has become a promising drug target. By suppressing LSD1 transcription in cancer cells, LSD1 inhibitors have demonstrated preclinical benefit, first in leukemia [12, 24] and more recently in carcinomas [48]. Moreover, LSD1 inhibitors have demonstrated benefit in combination therapies [3], including immunotherapies.

In particular, LSD1 inhibitors have shown preclinical potential in overcoming resistance to anti-PD1/PDL1 immune checkpoint inhibitors (ICIs) [6, 35, 40]. ICIs are among the most promising developments in cancer research of the past decade, as recognized by the 2018 Nobel Prize in Medicine. Despite this potential, the clinical reality is that typically up to 60% of patients show no response to single-agent ICI therapy [42, 47]. Overlapping factors contributing to resistance include lack of T cells at the tumor site, complementary immunosupressive mechanisms within the tumor microenvironment (TME), and other tumor-intrinsic features that enable immunoescape [42]. Moreover, in clinical combination therapies, ICIs are frequently administered concurrently with other treatments, with little regard to the dynamics of the immune response [47]. Sheng *et al.*demonstrated that LSD1 inhibition induces a type 1 interferon response, increasing T cell infiltration into the TME (Fig. 1). By knocking out LSD1 *in vivo*, they were able to overcome the poor immunogenecity of the B16-F10 melanoma cell line, increasing tumor infiltrating lymphocyte counts (TILs) and sensitizing the tumors to anti-PD1 treatment [40]. Similarly, Qin *et al.*combined clinical LSD1 inhibitors with anti-PD1 treatment in xenograft models of triple negative breast cancer [35]. They likewise found that LSD1 inhibition overcame the resistance observed in anti-PD1 treatment alone.

Modeling the dynamics of tumor growth and therapeutic response is a central focus of mathematical oncology, in which biological and biophysical knowledge is used to construct a model amenable to quantitative investigation. Among other possibilities, these models may offer a mechanistic explanation of existing data and generate new hypotheses, allow for the optimization of some experimental or clinical procedure, focus the scope or direction of future experiments, or inform a speculative, theoretical understanding of cancer-immune biology [11]. We refer to [11] for a recent review of mathematical models of immunology, and [10] for non-spatial modeling of tumor-immune dynamics. A broader overview of mathematical oncology can be found in [25, 44]. We briefly review the models that inspire our current work. Aligning with the data from [40], we specifically considered non-spatial ODE models.

The classic model developed by de Pillis *et al.*in [9] simulates immune-mediated tumor-growth as the interaction of three populations: tumor cells, natural killer (NK) cells, and CD8+ cytotoxic T cells. With only three equa-

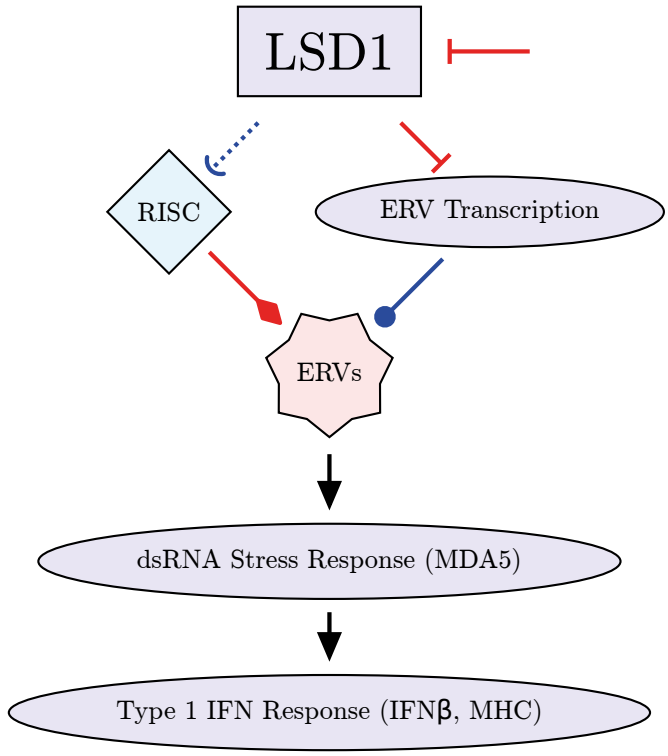

Fig. 1 The Proposed LSD1-Interferon Mechanism from [40]. LSD1 both suppresses transcription of endogenous retroviruses (ERVs) and regulates the RNA-induced silencing complex (RISC), which typically cleaves ERVs. Through both mechanisms, LSD1 inhibition enables ERV transcription and dsRNA accumulation. Through MDA5 and other sensors, dsRNA stress activates a type 1 interferon response in the cell, leading to tumor immunogenicity.

tions, this model is powerful in its versatility in capturing the dynamics of tumor growth under the influence of both innate and adaptive immune cytotoxicity. However, our focus in this work is on T cell dynamics specifically, since these are the populations most relevant to PD1/PDL1 checkpoint therapies and experimentally observed in [40]. Since the publication of the model [9] in 2005, much has been learned about the complex interplay between different CD4+ and CD8+ T cells populations. In particular, we wish to account for the complex management of T cell cytotoxicity by CD4+Foxp3+ regulatory T cells (Tregs).

Kim and Levy developed a model of the regulated adaptive immune response to antigen in [22] and [23]. Their model includes both naïve and mature compartments for antigen-presenting cells (APCs), CD8+ cytotoxic T cells, and CD4+ helper and regulatory T cells. A key feature of their model is the use of constant delay terms to account for the proliferative dynamics of T

cells. The immune dynamics in our model are inspired by this work, although we exclude both APCs and naïve cell populations.

Part of our work is motivated by that of Gadhamsetty *et al.*in [13, 14]. In these works, they used cellular Potts models to investigate cytotoxic T cell killing dynamics. Gadhamsetty *et al.*analytically derived their killing term for simple, monogamous killing regimes, and demonstrated *in silico* that this function extends to joint and mixed killing regimes [13]. The precise way in which we use this work is explained in Section 2.2.

The model presented in this work simulates the regulated T cell response to normal and LSD1-inhibited tumor growth, in order to further investigate the immunogenic and anti-tumor effects of LSD1 inhibition observed in [40]. This immunogenicity underlies the synergistic potential of LSD1-inhibitors combined with PD1/PDL1 ICIs.

The structure of this paper is as follows. In Section 2 we introduce our model, its underlying biological assumptions, the data we are using to fit it, and the alternative models considered. More technical detail is found in Appendix B. The results of our modeling are presented in Section 3. Our work suggests that LSD1 inhibition accelerates the anti-tumor T cell response, but does not necessarily enhance T cell cytotoxicity. Rather, LSD1 inhibition seems to reduce tumor tumor through other immune-mediated mechanisms. We provide diagnostics and validation for our model in Section 4, comparing it favorably to simpler alternatives. We also explore our model's robustness to the removal of data points. Concluding remarks are provided in Section 5.

2 Model and Methods

2.1 Model Overview

We model T cell-mediated tumor growth as a system of delayed differential equations, representing cancer and immune cell populations within the tumor microenvironment (Fig. 2). Our model has five state variables, (C, H, K, R, P), corresponding to tumor cells, helper and cytotoxic "killer" T cells, regulatory T cells (Tregs), and pro-immune cytokine. The model equations are:

$$\dot{C} = \underbrace{aC(1-C/\mu)}_{\text{Intrinsic Tumor Growth}} - \underbrace{k\psi(C,K)}_{\text{Cytotoxicity}}, \tag{1a}$$

$$\dot{H} = \underbrace{2^{m_H} s_H C^{\sigma_H}}_{\text{Recruitment}} - \underbrace{k\pi(C,H) + 2k\pi(C^{\rho_H}, H^{\rho_H})}_{\text{Proliferation}} - \underbrace{(d_H + r)H}_{\text{Death+Differentiation}} - \underbrace{kRH}_{\text{Regulation}}, \tag{1b}$$

$$\dot{K} = \underbrace{2^{m_K} s_K C^{\sigma_K}}_{\text{Recruitment}} - \underbrace{kPK + 2kP^{\rho_K} K^{\rho_K}}_{\text{Proliferation}} - \underbrace{d_K K}_{\text{Death}} - \underbrace{kRK}_{\text{Regulation}}, \tag{1c}$$

$$\dot{R} = \underbrace{rH}_{\text{Differentiation}} \underbrace{-kPR + 2kR^{\rho_H} P^{\rho_H}}_{\text{Proliferation}} - \underbrace{d_H R}_{\text{death}}, \tag{1d}$$

$$\dot{P} = \underbrace{p_H H + p_K K}_{\text{Cytokine Secretion}} - \underbrace{d_P P}_{\text{Decay}} - \underbrace{kP(R+K)}_{\text{Consumption}}, \tag{1e}$$

$$\psi(C,K) = \frac{\ell CK}{C+K+1}, \tag{1f}$$

$$\pi(C,H) = \frac{CH}{C+H+1}. \tag{1g}$$

In all equations, the superscripts correspond to the delay notation:

$$X^{\delta} = X(t-\delta).$$

The dimensionality of the populations in our model reflects the data provided by [40], which measures tumor volume (in mm^3). Tumor volume is proportional to tumor population, and there is little benefit in estimating cell numbers in the absence of more immune data. Rather, for any of the immune quantities present, we assume a scale comparable to the tumor volume. The population scales should be understood as approximating an effective proportionality, rather than absolute cell counts.

Note that our model has only a single compartment for pro-immune cytokine signalling, following the example in [22]. This variable primarily models the known functions of IL-2, e.g. from [31]. We acknowledge that many other pathways are involved in typical T cell dynamics. However, this simplification both limits model complexity while also allowing us to remain agnostic regarding the topology of extraneous signalling pathways.

Our construction of this model was not agnostic. Nonetheless, we compared it to simpler alternatives. We will consider the following three alternative models for tumor growth:

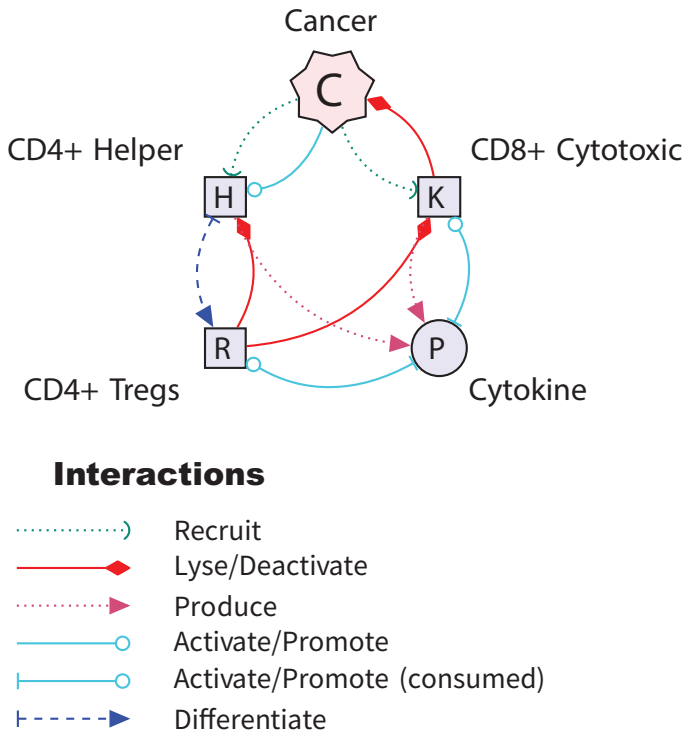

Fig. 2 Nonspatial Population Model of Immunosurveilled Tumor Growth. Our constant-delay ODE model of T cell-medaited tumor growth. The populations modeled are tumor cells (T), CD4+ helper T cells (H), CD8+ cytotoxic T cells (K), CD4+FOXP3+ regulatory T cells (R), and a simple pro-immune cytokine compartment (P).

$$\left.\dot{C} = \alpha C(1 - \frac{C}{\mu})\right\} \quad \text{Logistic Growth} \tag{2}$$

$$\left.\dot{C} = \alpha C \log\left(\frac{\mu}{C}\right)\right\} \quad \text{Gompertz Growth} \tag{3}$$

$$\left.\begin{aligned}\dot{C} &= \alpha C(1 - \frac{C}{\mu}) - CI \\ \dot{I} &= \beta C + \gamma IC - \theta I\end{aligned}\right\} \quad \text{Two Compartment} \tag{4}$$

For our results in Section 3, we simulate model (1) by solving Eqs. (1a)-(1e) numerically. The parameters used for model (1) are given in Table 1. A detailed discussion of parameter fitting and sensitivity is included in Section 4 and Appendix B.

2.2 Model Features and Assumptions

1. **Tumors intrinsically exhibit logistic growth.** The first term in Eq. (1a) models intrinsic tumor growth as logistic. We considered exponential, Gompertzian, and logistic forms of the growth term, and additionally considered a distinct linear death term for each. We fit these terms to the tumor growth data in immunodeficient (TCRα-KO) mice, from [40], in order to get a sense of the growth inherent to the tumor independent of the immune dynamics we seek to model. While other immunosuppressive mechanisms may still be active in TCRα-KO tumors, those are beyond the scope of our model. We found that the immunodeficient tumors were best modeled by logistic growth, with no distinct death term.
2. **Delayed T cell recruitment to tumor site following T cell development program.** In our model, both CD4+ helper and CD8+ cytotoxic T cells are recruited to the tumor microenvironment in proportion to the cancer population, represented in the first terms of Eqs. (1b) and (1b). The recruitment is delayed to account for the process of antigen-presenting cell (APC)-induced program of T cell development and proliferation, as developed in [22,23]. In [22], antigen stimulation activates APC cell maturation. APCs, in turn, migrate to the lymph node to activate the primary adaptive response, which develops according to a program of minimal development followed by APC-dependent expansion. Since we do not have any time series data for immune populations, we do not model this full process, excluding both APCs and naïve T cells. Nonetheless, for each population $X = H$ or K, we disentangle the parameters s_X, encompassing naïve T cell availability and stimulation rate, from the expansion multipliers 2^{m_X}. Here, m_X is the fixed number of divisions in the T cell development program. Since the time delay σ_X also depends on the number of divisions m_X, it is desirable to allow direction manipulation of the length and magnitude of the T cell development program in the model independently of the other influences on supply and recruitment dynamics. For our current work, we fix m_X to the values from [22].
3. **Helper T cells proliferate in dual-saturated response to tumor.** The second and third terms of Eq. (1b) model CD4+ helper cell proliferation dynamics. Our model assumes that CD4+ helper cells proliferate in response to APCs in the TME, a process which we simplify to a more direct cell-tumor interaction function π similar to the lysis function ψ, discussed further below. This saturation in the proliferative term has the added benefit of mimicking acquired immune resistance, including mechanisms mediated by the PD1 and CTLA4 immune checkpoints. Unlike CD8+ cells, IL-2 concentration does not seem to significantly modulate the proliferative TCR response in CD4+ cells [1]. Thus, in our model, the proliferative dynamics of CD4+ helper cells are uncoupled from the pro-immune signalling compartment. To account for proliferation time, the third term utilizes a constant delay ρ_H, set to 11/24, corresponding to an 11 hour cell cycle for CD4+ helper cells.

4. **Cytotoxic and Regulatory T cells proliferate in mass action response to pro-immune signalling.** The second and third terms in Eqs. (1c) and (1d) represent the proliferative dynamics of activated CD8+ and Treg populations. Our model assumes that, unlike CD4+ helper cells, CD8+ cytotoxic and CD4+ regulatory cells proliferate via cytokine signalling, according to a simplified mass action law. IL-2 modulates the proliferation of activated CD8+ population, without significant dependency on further stimulation [1, 19]. By contrast, low concentrations of IL-2 instead promote the differentiation of memory phenotype in naïve CD8+ cells, observed both *in vivo* during viral infections [19] and *in vitro* during chimeric antigen-receptor (CAR) T cell expansion [18]. We acknowledge that despite many *in vitro* experiments suggesting the necessity of IL-2 for the expansion of CD8+ cytotoxic cell response, it has been observed, *in vivo* for IL-2R KO mice, that there seem to be redundant mechanisms for CD8+ proliferation [19]. As for Tregs, IL-2 has been well-documented as essential for peripheral Treg function and expansion [5]. The induction of Tregs by low-dose IL-2 has emerged in recent years as a promising new treatment for autoimmune disease [49]. As an additional modeling benefit, the structure we use captures cytokine competition between CD8+ cells and Tregs as a distinct mechanism of immunosuppression, due to the fourth and fifth terms in Eq. (1d). This is supported by the the work of Chinen *et al.*, which suggests that IL-2 competition is a significant component of Treg-driven control of CD8+ populations, but not CD4+ populations [5]. Further, by using an identical, non-saturated proliferative mechanism for CD8+ and Treg populations, by design allowing them to proliferate at a greater rate than CD4+ helper cells post tumorigenesis, our model dynamics align with the proliferative patterns observed experimentally in [40]. Sheng *et al.*found both Tregs and cytotoxic cells to be more proliferative than helper T cells. At day 14, they found that up to 70% of Tregs and 60% of CD8+ cells expressed the proliferative marker Ki67+, compared to only 30% of helper CD4+ cells. We assume CD4+ regulatory cells have the same 11-hour proliferation time as helper cells (ρ_H), while CD8+ cells have a proliferation time (ρ_K) of 8 hours [1].
5. **Helper and cytotoxic T cells produce inflammatory cytokine.** Our model assumes that helper T cells are primarily responsible for pro-immune signalling, although CD8+ cytotoxic cells also produce pro-inflammatory signals. Both populations produce cytokine at fixed linear rates p_H, p_K. For our present study, we fix these values to those from [22]. Thus, for the moment, the dynamics of cytokine signalling in our model is rigidly contingent on those of the other compartments. However, we expect the interferon response induced by LSD1 inhibition to alter the dynamics of the signalling compartment. We leave this for future work.
6. **Differentiation of helper T cells into Tregs.** In our model, CD4+ helper cells differentiate into CD4+ Tregs at a fixed rate r, similar to the Treg dynamics from [22]. Our model does not distinguish between peripheral iTregs and thymal nTregs. We note the mechanisms of peripheral

Treg differentiation are still unclear, as is the degree of plasticity between helper and regulatory CD4+ cell lineages [27].

7. **Decay of Immune Populations.** We assume that CD4+ helper and regulatory cells and CD8+ cytotoxic cells deactivate at fixed linear rates: d_H for both CD4+ populations and d_K for CD8+ populations. Further, positive growth signal decays at rate d_P. We take these rates from [22].
8. **Cytotoxic T cells lyse tumor cells with double-saturated sigmoidal dynamics.** The second term in Eq. (1a) represents anti-tumor cytoxicity from CD8+ T cells. Saturated kill terms for T cell cytotoxicity are standard in the literature [10]. more generally, sigmoidal functional forms are typical for immune response to antigen, and have been used, for instance, to faithfully model Potts-type lattice simulations of TCR-pMHC binding dynamics [51]. It is desirable to use a function that saturates with respect to both tumor and immune populations, as such a property allows the function to handle the dynamics of both tumor growth and collapse. We take our function from the work of Gadhamsetty *et al.*, which simulates T cell cytotoxicity in a Potts model framework [13, 14]. They heuristically derive a similar function when T cells follow a monogamous killing regime, and demonstrated *in silico* that the function extends to joint and mixed killing regimes [14].
9. **Kinetic coefficient.** All terms representing cell interactions in the TME are multiplied by a kinetic coefficient, k. Adjusting this coefficient affects the speed of population transitions in the transient immune dynamics. For our current study, we fix k to a constant value of 10.

Our model has several limitations worth highlighting. We excluded these dynamics due to their practical unidentifiability in this current work. In particular, as discussed above, we excluded T cell exhaustion, checkpoint-mediated immune tolerance, the innate immune response, and myeloid cell dynamics.

2.3 Experimental Data

For data, we used three of the experimental data sets from [40]. First, our target for modeling was the experimental data set corresponding to [40, Fig. 5E] which measured the tumor growth in 28 individual B16 murine xenografts. These are divided into 4 experimental conditions of CRISPR gene silencing: LSD1-KO, MDA5-KO, LSD1+MDA5-DKO, and a scramble control ($N = 7, 7, 6, 8$, respectively). Note that, as described in Fig. 1, MDA5 is an important mediating component for the pro-immunity interferon response produced by LSD1 inhibition, and the mechanism of focus in [40]. Thus, our work, we are looking for consistent differences between the LSD1-KO condition and both the control and LSD1+MDA5-DKO conditions, which would implicate the LSD1-IFN axis. In addition to this target data set, we also make use of some of the growth data from [40, Fig. 5C] corresponding to scramble and LSD1-KO tumors within immunodeficient TCRα-KO mice. Finally, in Fig. 4, we use the flow cytometry T cell counts from [40, Fig. 6A] in Fig. 4 in order

Table 1 Model Parameters. Parameter values replaced with an asterisk (*) were estimated individually for each mouse model.

	Parameter Name	**Description**	Value	Reference
a	Tumor growth rate	Controls tumor-intrinsic logistic growth	*	estimated
d_H	CD4+ Death Rate	Linear death rate for CD4+ helper and regulatory T cells	0.23	[22]
d_K	CD8+ Death Rate	Linear death rate for CD8+ cytotoxic T cells	0.4	[22]
d_P	Cytokine Decay Rate	Linear decay rate for IL-2	5.5	[22]
k	Kinetic Coefficient	Controls rate of immune interactions in the TME	10	fixed
ℓ	Immune-tumor Lysis Parameter	Controls CD8+ T cell cytotoxicity in kill function $\psi(C, K)$	*	estimated
μ	Tumor carrying capacity	Limits tumor-intrinsic logistic growth	*	estimated
m_H	CD4+ Developmental Divisions	Number of CD4+ cell divisions in APC-driven development program in lymph node	2	[22]
m_K	CD8+ Developmental Divisions	Number of CD8+ cell divisions in APC-driven development program in lymph node	7	[22]
p_H	CD4+ Cytokine Secretion	Controls production of IL-2 by CD4+ helper T cells	100	[22]
p_K	CD8+ Cytokine Secretion	Controls production of IL-2 by CD8+ T cells	1	[22]
r	Treg Differentiation Rate	Fractional rate at which CD4+ helper cells differentiate into Tregs	*	estimated
ρ_H	CD4+ Division Time	Length of cell cycle for proliferating CD4+ helper and regulatory T cells	11 hr	[8]
ρ_K	CD8+ Division Time	Length of cell cycle for proliferating CD8+ cytotoxic T cells	8 hr	[8]
s_H	Supply rate of CD4+ cells	Controls delayed supply of CD4+ cells to TME in response to tumor antigen	*	estimated
s_K	Supply rate of CD8+ cytotoxic cells.	Controls delayed supply of CD8+ cells to TME in response to tumor antigen	*	estimated
σ_H	CD4+ Development Time	Length of APC-driven CD4+ T cell development program in lymph node (divisions $\times$ doubling time)	1.46 days	[22]
σ_K	CD4+ Development Time	Length of APC-driven CD4+ T cell development program in lymph node (divisions $\times$ doubling time)	3 days	[22]

to provide circumstantial evidence for an earlier onset of the immune response in LSD1-KO tumors.

3 Results

We simulate

3.1 Immune Response Accounts for Interrupted Tumor Growth

Many of the mouse tumors from [40] have irregular growth in the second or third week, usually in the 10-15 day range. A similar pattern can be observed in other subcutaneous B16 models in [17,26,45]. After a week or two of tumorigenesis and steady growth, the tumor stagnates or even regresses for a few days. Then, in typical B16 tumors, growth resumes, often at an accelerated rate. By design, our model hypothesizes that we can account for this irregularity via the tumor's interaction with the primary adaptive immune response.

As described in Section 2 and Appendix B, we opted to parameterize independently for each tumor growth time series. In most tumor-specific simulations of the immune response, a stereotypical script emerges, as seen in Fig 3. Both helper and cytotoxic T cells are recruited to the tumor site, although helper T cells are usually recruited more quickly. Helper T cells proliferate when stimulated by the tumor cells, and release pro-immune cytokines, including IL-2. These cytokines stimulate cytotoxic T cell proliferation, inducing significant cytotoxicity that interrupts steady tumor growth. Note that this pattern conforms to the B16 immune data from [34], which saw CD4+ helper cells peak a few days before CD8+ cytotoxic cells. The helper T cell population differentiates into Tregs at a fixed rate, and regulatory cells likewise proliferate in the presence of pro-immune signalling. The regulatory T cells deactivate both the helper and cytotoxic populations while consuming most of the remaining pro-immune signal for their own proliferation. Once Tregs dominate the immune populations, tumor stagnation ends and growth resumes.

3.2 Simulated Immune Response Activates and Peaks Earlier in LSD1-KO Tumors

In our simulations, both the CD4+ helper and CD+8 cytotoxic cell populations tended to reach their peak earlier in the LSD1-KO condition, compared to both control and LSD1/MDA5 DKO tumors. On average, helper cells reached their maximal helper (cytotoxic) T cell population at day 14.01 (14.2), while control and DKO tumors peaked at day 17.11 (16.68) and 18.53 (17.62), respectively (Fig. 4, **A-B**). However, after adjusting for multiple testing, only the difference in timing between LDS1-KO and LSD1/MDA5 DKO tumors rises to statistical significance in our small sample. Even so, this agrees well with a separate experiment from [40] under similar experimental conditions, in which flow cytometry revealed elevated levels CD4+ and CD8+ T cells in LSD1 KO tumors on day 14, relative to control and DKO tumors. (Fig. 4**D**, or Fig. 6**A** from [40]).

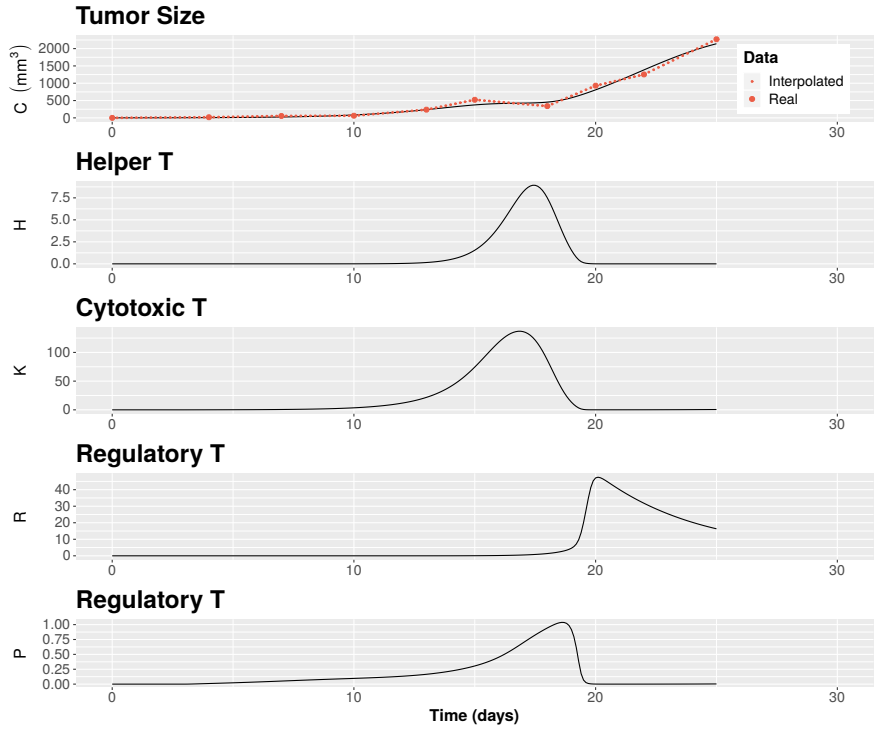

Fig. 3 Simulations of Immune-Mediated Tumor Growth. Our model (black) infers an underlying adaptive immune response as responsible for temporary tumor growth stagnation, from linearly interpolated tumor growth data (red) from [40]. The graphs, from top to bottom, show simulated dynamics over 30 days for tumor volume, CD4+ helper T cells, CD8+ cytotoxic T cells, CD4+FOXP3+ regulatory T cells, and pro-immune cytokine.

We emphasize that this difference appears only in LSD1-KO tumors where the dsRNA sensor MDA5 has not likewise been knocked out. Thus, our model suggests that the LSD1-dsRNA-IFN axis under investigation in [40] accelerates the anti-tumor T cell response.

Interestingly, our model not demonstrate an increase in effective cytotoxicity under LSD1 inhibition. At the time of peak immune response, we simulated no difference in the fractional kill rate ($C^{-1}\psi$ in our model, Eqs. 1a,1f), as seen in Fig. 4**D** and Fig. 5. This coincides with unpublished experimental evidence collected by Sheng et al. that LSD1 inhibition does not enhance the cytotoxicity of individual T cells. Moreover, as noted in [40], RNAseq revealed that PD-L1 was upregulated in LSD1-KO tumors, possibly suppressing the anti-tumor immunity of CD8+ T cells. This agreement between model and experiment furhter supports the notion that LSD1 inhibition does not directly enhance anti-tumor cytotoxicity. The significantly retarded tumor growth in LSD1 inhibited tumors, as observed in [40] and [35], must be attributed to other factors. Nonetheless, the process is likely to be immune-mediated, given

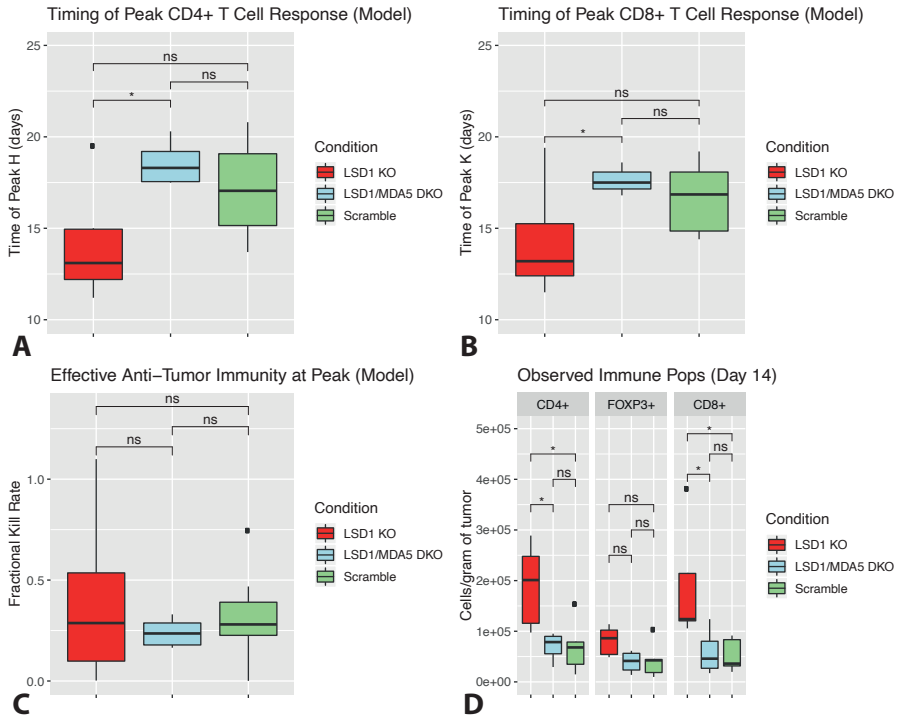

Fig. 4 Inferred Dynamics of T Cell Response. In subfigures (A) and (B), we present the time (days post-tumor injection) at which the CD4+ helper and CD8+ cytotoxic T cells reach their maximum population within our model, grouped by experimental condition.

the rescuing effect of MDA5 inhibition. Further, if LSD1-inhibition reduces T cell cytotoxicity through a mechanism besides the upregulation of PD-L1, then countering that mechanism and restoring full CD8+ functionality would maximize the effect of combination anti-PD1 therapy.

3.3 Growth Dynamics

As noted in Section 3.2, the simulated cytotoxicity in our model suggests that LSD1 inhibited tumors see a quicker onset of the adaptive immune response, accounting for the increased number of tumor infiltrating lymphocytes. However, this does not convincingly account for the decreased tumor growth observed LSD1-KO tumors.

Beyond the immune dynamics incorporated into our model, LSD1 inhibition appears to slow tumor growth via other mechanisms. We see that, despite comparable distributions for the carrying capacity parameter μ, the tumor growth rate parameter α is lower for LSD1 KO tumors, compared to both control and LSD1/MDA5 DKO tumors. In our model, this difference manifests in early tumorigenesis, when tumor volume is well below capacity and

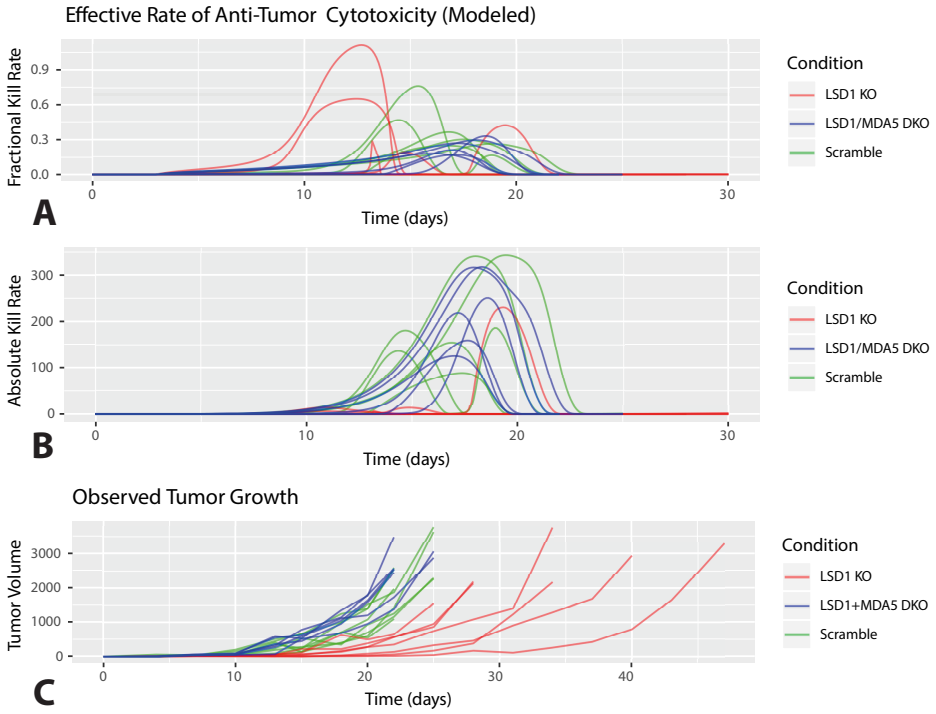

Fig. 5 Effective Anti-Tumor Immunity in Model. In subfigures (**A**) and (**B**), we present the simulated fractional and absolute kill rates (in our model, $C^{-1}\psi(C,K)$ and $\psi(C,K)$, respectively) over time. We do not see any consistent and appreciable difference indicating that LSD1 inhibition increases anti-tumor immunity. For comparison, we include the observed tumor growth data from [40], which demonstrates an appreciable reduction of tumor-growth (**C**).

growth is approximately exponential with rate α. Thus, when we remove T cell dynamics, our model still has LSD1 KO tumors growing more slowly *in silico* (see Fig. 6). Interestingly, this pattern does not appear in the immunocompromised mice from [40]. When Sheng *et al.*used mice without functioning T cell receptor alpha (TCRα), they observed no difference in growth between LSD1 KO and control tumors. Similarly, when we fit the logistic growth model to the TCRα-KO data (Fig. 6D, Table 3), we do not observe the difference captured in our T cell free model for immunocompetent mice.

Assuming that our model captures T cell dynamics accurately, we consider two non-mutually-exclusive explanations for the 'intrinsic' reduction in tumor growth within our model. First, our system does not comprehensively model tumor-immune cytotoxicity. For instance, natural killer (NK) cells and memory T cells are not accounted for in our model. Another possibility is that tumor growth mechanisms themselves may be slowed by LSD1 inhibition, mediated by the MDA5-dsRNA-immune stress response.

It is possible that the reduction in the growth parameter is at least partially accounted for by the presence of continuous cytotoxic immunity not otherwise included in our model. Indeed, RNAseq analysis in [40] found the innate immune response to be upregulated. Innate cytotoxicty from, e.g., NK cells, is not included in our model. The nature of model (1) is to specifically capture the rapid-onset, well-regulated adaptive response to antigen. Although regulatory T cells do suppress NK cells in the TME [4], the timing for this will not align with the immune dynamics of our model. Moreover, T cell cytotoxicity itself is not limited to the sharp onset-regulation dynamic of our model. Our work emphasizes peak T cell response, at the cost of both ongoing and memory T cell dynamics, which are less clearly understood [46].

To explore this possibility, we could examine the two compartment model (4), which, unlike our primary model, allows for sustained cytotoxicity. We do see that that the difference in the growth parameter α between LSD1-KO and control tumors is no longer significant in the two compartment model, despite a greater magnitude (Fig. 6E). Nonetheless, we have reason to suspect the ability of the two compartment model to capture T cell-independent tumor growth. Inspection reveals that the two compartment model has a tendency to estimate relatively high growth rates that do not, qualitatively, resemble tumor growth in TCRα-KO mice (Fig. 6F). In particular, the two compartment model tends to predict a higher rate of unencumbered tumor growth than we observe both when we fit a logistic growth model to immune-compromised (TCRα-KO) mice, and when we fit our other models to the primary dataset of immunocompetent mice (Fig. 9).

We consider also tumor-intrinsic explanations for the reduced growth parameter. We considered EMT- and CSC-related pathways, looking at the RNAseq data from [40], and found no convincing evidence for them. Alternatively, we consider that a major limiting factor on growth is proper tumor angiogenesis. There is evidence that LSD1 regulates angiogenesis [20]. The RNAseq data from [40] suggests that the Notch pathway is activated in LSD1 KO tumors (Fig. 7). Notch regulates angiogenesis via the VEGF pathway, bal-

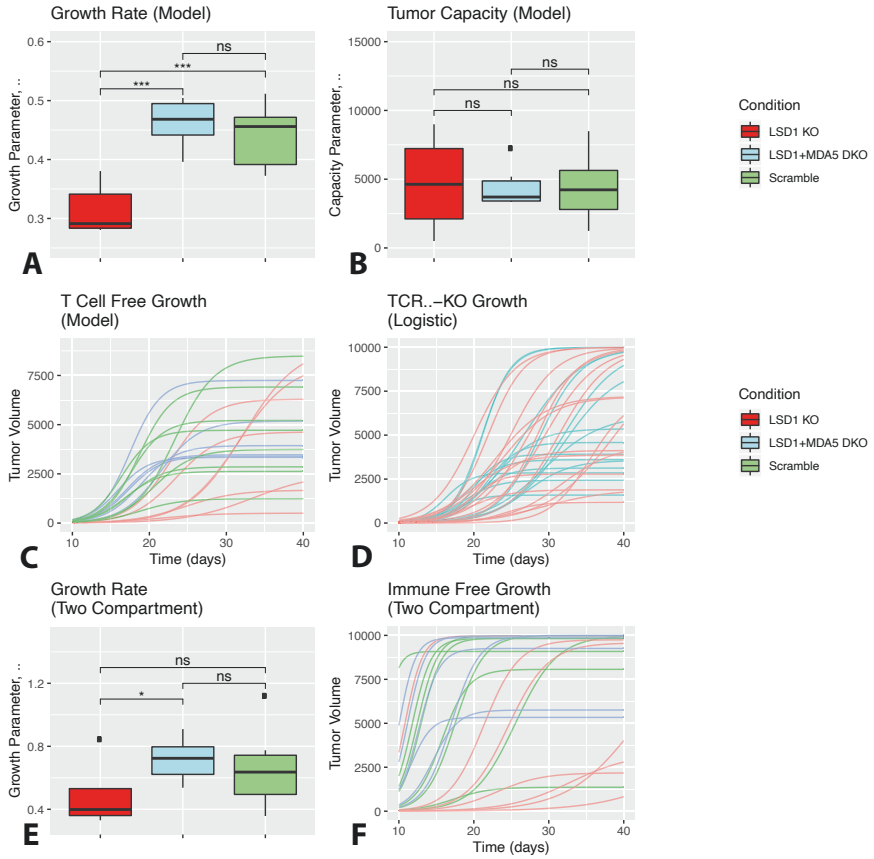

Fig. 6 T Cell Dynamics Alone Do Not Fully Account for Slowed Tumor Growth in LSD1 KO Tumors. We present the T cell-independent growth dynamics of our model. In the top two figures, we present the values of the model parameters for intrinsic growth (**A**) and tumor capacity (**B**). In (**C**), we simulate T cell free tumor growth by eliminating immune cell dynamics from our parameterized model (i.e. reducing our model to logistic growth with parameters a, M_C). We see that, despite comparable carrying capacities, the LSD1 KO tumors seem to exhibit slower 'intrinsic' tumor growth, separate from the model's T cell dynamics. This suggests that the anti-tumor effects of LSD1 inhibition include the innate immune response and/or tumor-intrinsic factors. Since this pattern is not observed in TCRα KO tumors (**D**, fit to simple logistic growth curves, see Table 3), the T cell response is still implicated as a mediator, in either case.

ancing tip and stalk cell populations in the fomration of new blood vessels. Its effect on tumor angiogenesis is context-dependent, e.g. [28] vs [38]. Recently, Augurt *et al.*found that LSD1 inhibitors reactivate the Notch pathway in small cell lung cancer, inhibiting tumor growth [2]. In the *in vivo* data collected by Sheng *et al.*, we see that the Notch activation in LSD1-KO tumors is less pronounced in LSD1/MDA5-DKO tumors. Moreover, Notch was not activated *in vitro*. This suggests the possibility that the LSD1-dsRNA-interferon

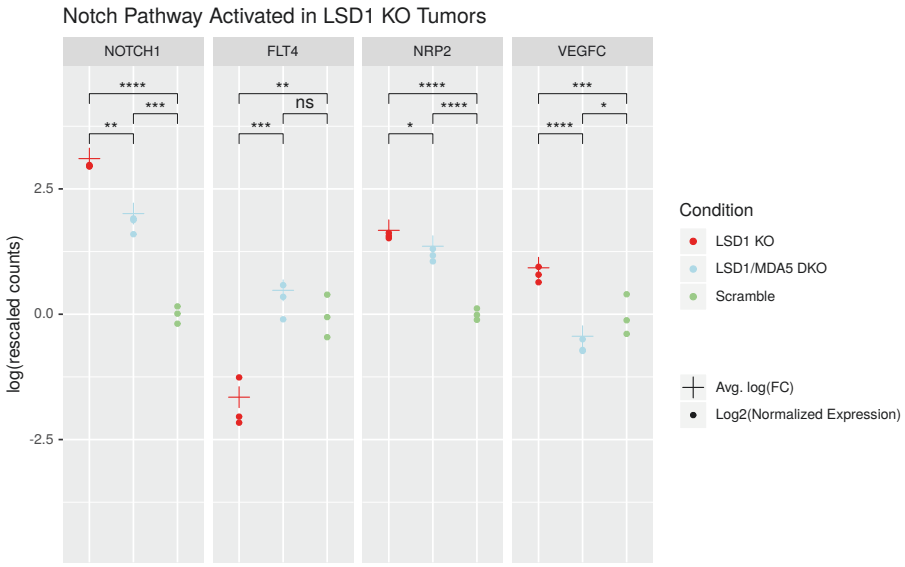

Fig. 7 Notch pathway upregulated *in vivo*. NOTCH1 is upregulated *in vivo*, but not *in vitro* (not shown here), for LSD1 KO tumors, and VEGF-r4/FLT4 was downregulated. This could potentially affect angiogenic sprouting, as in [41,43]. Dots represent pre-processed $\log_2$ counts from [40], rescaled by the average for the scramble control, and pluses represent the estimated average $\log_2$FC, after smoothing and normalization. We assessed differential gene expression among all significantly expressing genes, as described in Appendix A

axis induces Notch activation, which could restrain tumor growth. However, the significance of Notch activation to anti-tumor LSD1 inhibition remains unclear.

4 Model Fitting and Diagnostics

4.1 Model Fitting and Validation

For the DDE model described in Section 2.2, Eqs. (1a)–(1g), we adapted many of the parameters from [22], and fixed the kinetic coefficient k at an arbitrary value. Thus, for the purposes of model fitting and validation, we limit our degrees of freedom to six parameters: tumor growth parameters α, μ, immune recruitment parameters s_K, s_H, the cytotoxicity parameter ℓ, and the rate of Treg differentiation r. The full list of model parameters is given in Table 1.

For the one-dimensional models (2) and (3), we allowed our initial condition C_0 to vary as a third parameter. For our main model (1) and the two compartment model (4), we used a uniform initial condition for all tumors. All immune populations were initialized at 0. For the main DDE model (1), we assumed all state variables were 0 for $t < 0$.

For the one-dimensional curves, our models become the closed-form solutions of the logistic and Gompertz equations. For our main model (1) and the two compartment model (4), we solved our equations numerically. We fit our model parameters using a Markov chain Monte Carlo, taking the point-estimates from the posterior distribution. We linearly interpolated our data prior to fitting. More details are provided in Appendix B. Figure 12 provides a visualization of the prior and posterior distributions for one of our fittings. As can be seen, although the posteriors are sometimes multimodal, the model is locally identifiable.

We compare our model to the alternatives by computing the Bayesian Information Criterion (BIC) for each model, using the point-estimated parameters (Fig. 8). A lower BIC indicates a more explanatory and/or parsimonious model. Using a signed rank test, we found that our model was generally favored over all three of the alternatives (Fig. 8). Unsurprisingly, model (1) was heavily favored over the logistic and Gompertz models, with a mean BIC improvement of -40.2 and -40.3, respectively. More importantly, for 17 of the 28 tumors, model (1) was preferred to the two compartment model (4), albeit with a more modest mean difference of -3.4. For 5 tumors, the magnitude of BIC improvement was greater than 10, while for only one tumor was (4) preferred by more than 4.

As an additional point of comparison, we consider the model-inferred rates of intrinsic tumor growth. Both models (1) and (4) assume that, in the absence of competitive immunity, tumor growth is logistic. Thus, parameterizing each involves estimating a rate of 'intrinsic' growth apart from the model's immune dynamic. To validate these estimates, we can use the tumor growth data from immunodeficient (TCRα-KO) as a rough experimental proxy of immune-free growth. As previously discussed in Section 3.3 and Fig. 6F, we fit logistic growth to the TCRα-KO mice tumors. In Fig. 9, we compare the growth rates of models (1), (2), and (4), fit to our primary data set, to the growth rates estimated for the TCRα-KO data. We see that the two compartment model tends to estimate much higher growth rates than those estimated for the immunodeficient control. By contrast, the primary model estimated growth rates comparable to those of the TCRα-KO tumors. That is to say, they were not statistically differentiable.

4.2 Model Sensitivity (Data Removal)

We examined the robustness of our model fitting to the exclusion of key data points. To that end, we examined two specific time series from out data set: tumor growth data from a control tumor and from an LSD1 KO tumor. For each, we considered two modifications to the data.

First, for each time series, we removed an intermediate interval of data corresponding to a single irregular observation. We chose the removed observation to be one that suggests a period of particularly irregular growth and stagnation. This allows us to consider the possibility that an interruption in

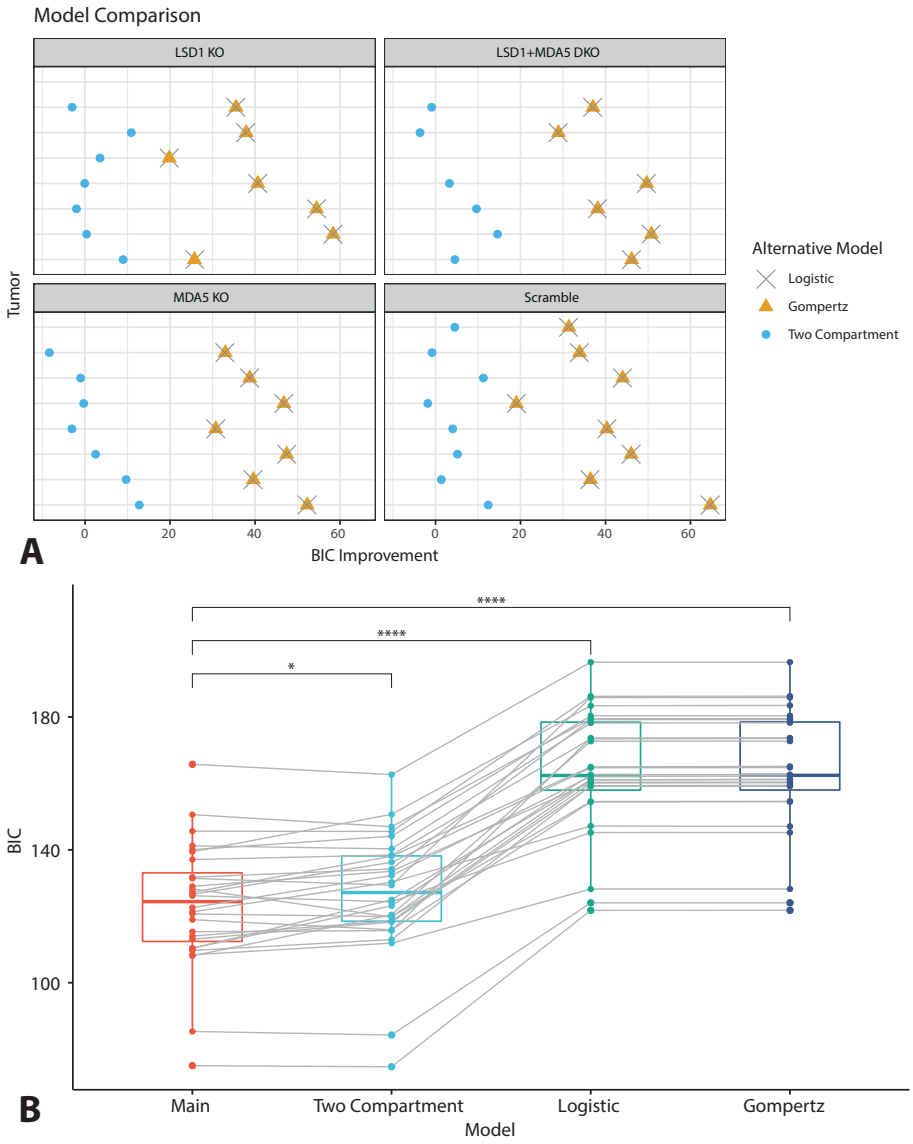

Fig. 8 Model Comparison For each of the 28 tumors, we computed the the BIC to evaluate the relative performance of our model versus simpler alternatives. In **A**, for each tumor time series from [40], we compare our model (1) to each alternative, i.e. $\mathrm{BIC}_{\mathrm{Alt}} - \mathrm{BIC}_{\mathrm{Main}}$. In **B**, we compare the alternatives to (1) as paired populations, using the Wilcox signed rank test and adjusting for multiple testing. We see that our primary model significantly improves on the three alternatives, although the improvement is typically modest when we consider the two compartment alternative.

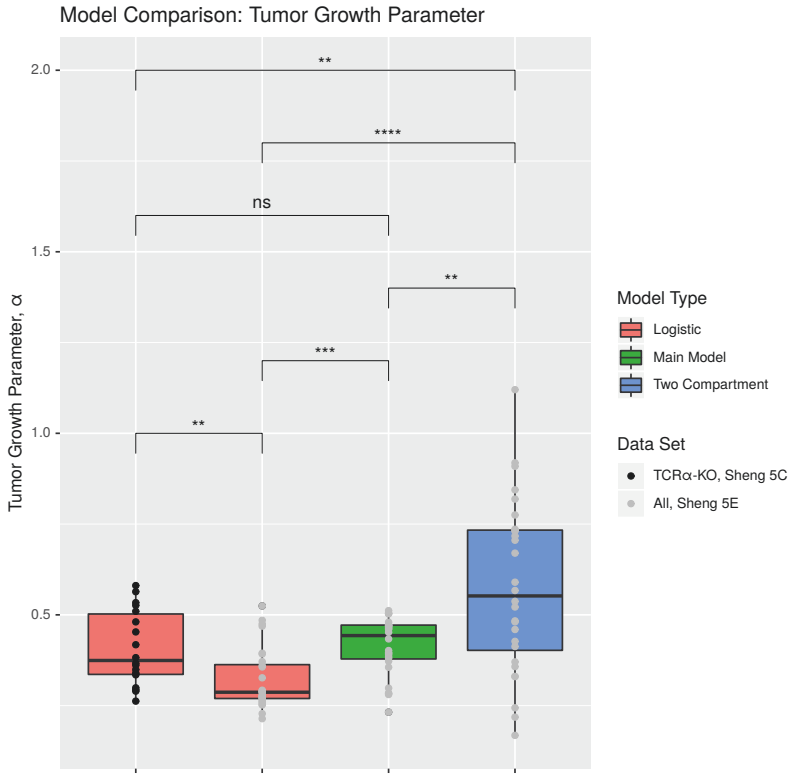

Fig. 9 Tumor Growth Rate Estimates in Immunodeficient and Incompetent Mice. We compare the estimated value of the tumor growth parameter α for immunocompetent mice, using models (1), (2), and (4), to those rates estimated from the tumors in TCRα-KO mice, using model (2).

growth, which our modeling attributes to T cell cytotoxicity, is instead due to a 'blip' of errorful measurement. This is key to the validity of our current work.

Second, for each time series, we removed the last two observation (and the associated interpolated points). This allows us to examine the forecasting potential of our model and its ability to recover the dynamics of immunoescape and tumor recovery from early growth data. Forecasting future growth was not the objective of our present modeling work. Nonetheless, it is an informative test of the limitations of our model.

In Fig. 10, we present the result of this first modification to our model fitting. For both data sets, we see that removing an interval of irregular growth does not affect the timing of the immune response. The intensity of the immune reaction decreases, somewhat, as a smoother, more regular trajectory is fit to the missing interval. This is seen with particular clarity in the LSD1-KO tumor data. The timing of the peak T cell reaction is robust to the removal of the

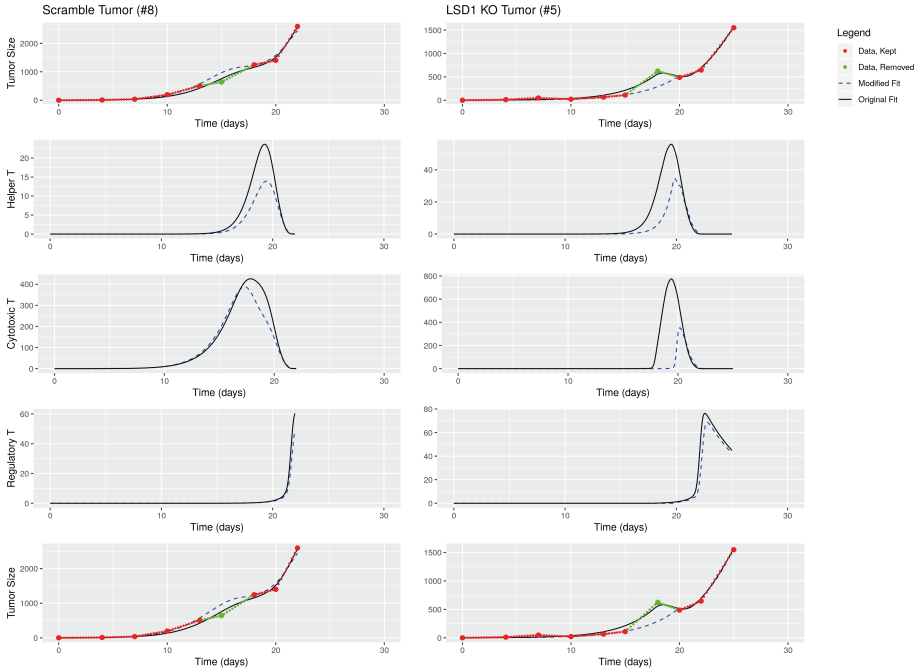

Fig. 10 Model Refitting after Data Exclusion (Intermediate Interval). We present the original and modified fittings of model (1) for two of our time series. For the modified fitting, we excluded one intermediate real observation and the associated interpolated points, shown in green to distinguish from the remaining (red) data points. For the scramble control (LSD1-KO) tumor, we excluded all points between days 13 and 18 (15 and 20).

observation at day 18, indicating that more than a single outlying observation is suggestive of significant tumor stagnation. Though the biological mechanism assumed by our model is hypothetical, our inference of immune dynamics seems robust.

In Fig. 11, we present the result of the second modification to model fitting, in which we truncate the final few days of tumor growth. The two data sets under consideration demonstrate qualitative different sensitivities to this exclusion. For the scramble control tumor, the exclusion of the final data points leads to a fitting in which the final remaining data point is close to capacity. Thus, the projected future growth levels out. This a significant divergence from both the actual data and the original fit. In contrast, for the LSD1-KO time series considered, the projected future growth still reasonably resembles future data. We additionally note that, for the control time series, the entire timing of the estimated immune response is shifted to an earlier window. For the LSD1-KO tumor, the timing of the immune response remains the same. Taken together, our model does not show itself to be a reliable tool for future growth forecasting.

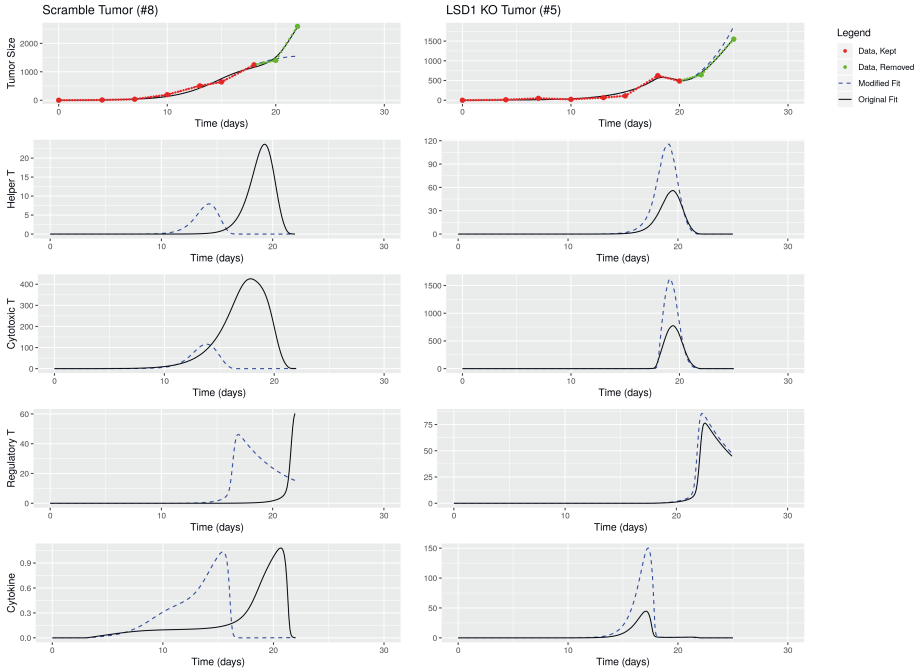

Fig. 11 Model Refitting after Data Exclusion (Final Data). We present the original and modified fittings of model (1) for two of our time series. For the modified fitting, we excluded the final two real observations and the associated interpolated points, shown in green to distinguish from the remaining (red) data points. For the scramble control (LSD1-KO) tumor, we excluded all points after day 18 (20).

5 Discussion

We created a simple mathematical model of the adaptive immune response to tumor growth in order to infer the potential effects of LSD1 inhibition on T cell dynamics. Our model suggests that LSD1 inhibition does accelerate tumor infiltration of T cells, via the MDA5-mediated interferon response studied in [40]. We further found that, despite increased levels of tumor-infiltrating T cells observed at day 14 *in vivo*, our model does not imply that LSD1 inhibition alone increases the instantaneous rate of T cell cytotoxicity in TME. This suggests that the synergistic effect of combination anti-LSD1/anti-PD1 treatment observed *in vivo* in [35, 40] is not due to additive anti-tumor effects. Rather, our modeling suggests that any benefit of LSD1 inhibition to effective anti-tumor T cell cytotoxicity occurs PD1/PDL1 is likewise targeted. However, as previously observed in [40] and [35] and discussed in Section 3.3, we still have that LSD1 inhibition reduces tumor growth. Moreover, this reduction is eliminated when MDA5 is also knocked out, implicating the interferon response from [40] and, by extension, the immune system.

It is unclear why the increased level of T cells in LSD1-inhibited tumors may not translate to increased cytotoxicity. As we have noted, [40] found the PDL1 was upregulated in LSD1-KO tumors. However, we briefly consider alternative mechanisms. LSD1 inhibition both induces an IFN-β response and upregulates TGF-β. IFN-β is commonly used to reduce autoimmunity in multiple sclerosis [21, 50], inhibiting memory T cell activation. It is possible that the type 1 inteferon response sustaining T cell activity in the TME of LSD1 KO tumors is simultaneously suppressing elements of anti-tumor immunity. Alternatively, the upregulation of TGF-β may also reduce activation, proliferation, and/or cytotoxic function in CD8+ cells [30,33]. Despite its potential to increase and sustain T cell infiltration, if LSD1 inhibition can simultaneously undermine anti-tumor immunity in the TME, the mechanism responsible needs to be identified for effective therapeutic targeting. Given two tumors with distinct immune profiles, it is entirely plausible that LSD1 inhibitors could sensitize one to checkpoint therapies, while disabling immunosurveillance in the other.

In future work, we intend to investigate and model the effect of LSD1 inhibition on many tumor-immune mechanisms currently excluded from the model. The effect of LSD1 inhibition on the mechanisms PD1-mediated immune tolerance is still unclear. Additionally, our current work does not consider myeloid cell dynamics. Recent work suggests that LSD1 promotes immunosuppressive myeloid cells, and that its inhibition reduces the differentiation of these populations in the TME. Condamine *et al.*found that LSD1 inhibitors reduced the differentiation of myeloid derived suppressor cells (MDSCs) and polymorphonuclear (PMN) cells *in vitro* and *in vivo*, synergistically enhancing the effect of anti-PDL1 agent [6]. With the appropriate data, we hope to later explore the dynamic interplay between myeloid and T cell populations in the TME under the effect of LSD1 inhibitors, clarifying the tumor-immune signatures favorable to anti-LSD1/anti-PD1 combination therapy. Finally, more investigation is warranted into T cell exhaustion in LSD1 inhibited tumor-immune systems. While LSD1 inhibition increases T cell tumor infiltration, complementing anti-PD1 treatment in the short-term, we cannot discount the possibility that an LSD1-mediated interferon response might also accelerate other (non-PD1) forms of T cell exhaustion. This would have serious implications for the long-term efficacy of LSD1 inhibitors as compliments to immunotherapy.

Acknowledgements

We would like to thank Heyrim Cho and Asia Wyatt for helpful discussions in drafting this paper. The work of JM was supported in part by the COMBINE Fellowship under NSF award DGE-1632976. The work of DL was supported in part by the National Science Foundation under Grant Number DMS-1713109.

A Statistical Comparisons in Figures

For the pairwise comparisons in Figs. 4, 6, 8, and 9, we used an unpaired Student's t-test. For each panel, we applied a Benjamini-Hochberg adjustment for multiple-testing. In order to validate the chocie of a t-test, we used the Shapiro-Wilk test for normality. We cannot reject normality for the samples in Figs. 4, 6, and 8 ($P > 0.05$). For Fig. 9, two of the samples were somewhat non-normal. Left to right in 9, the S-W statistic had values $0.93, 0.85, 0.90, 0.98$ corresponding to $P = 0.17, 8.8e-4, 9, 0.010.81$. We used the same comparison for Fig. 4**D** as in [40].

For the differential gene expression (DGE) analysis for Fig. 7, we used the gene counts from [40] (data accessible at NCBI GEO database, accession GSE112230), and the R package `edgeR`. We normalized the counts using the TMM method, and removed minimally expressing genes, leaving us with 12305 genes remaining. We fit a linear model to compare gene expression between the three experimental tumor conditions: scramble control, LSD1-KO, and LSD1/MDA5 DKO tumors. Our workflow was based upon the tutorial in [7]. When adjusting for multiple testing, we used the BH method as before, and adjusted for all three pairwise contrasts (between our experimental conditions) for the full set of expressing genes, together.

B Description of Statistical Model and MCMC Fitting

Consider the tumor growth data for tumor i as a time series $\boldsymbol{y}_i = (y_i(t_j))_{j=1}^{n_i}$. We assume a statistical model of the form

$$y_i(t) = f(\boldsymbol{p}_i, t) + \epsilon_i(t) \tag{5}$$

$$\epsilon_i(t_1), ..., \epsilon_i(t_n) \sim_{\text{iid}} N(\mu_i, \sigma_i) \tag{6}$$

where $f(\boldsymbol{p}_i, \cdot)$ is a deterministic model and $\epsilon_i(\cdot)$ is the measurement noise, parameterized by $\boldsymbol{p}_i, \mu_i, \sigma_i$ individually for each tumor time series i. The model $f(\boldsymbol{p}_i, \cdot)$ is the solution to either our main DDE model (1) described in Section 2.1, (1), or one of the alternative ODE models in Section 2.1 (2, 3, 4). We use $\boldsymbol{f}(\boldsymbol{p}_i)$ to denote $(f(\boldsymbol{p}_i, t_j))_j$, i.e. the estimated time series from our model, corresponding the data $\boldsymbol{y}_i$. For our measurement noise, we ideally would have $\mu_i = 0$ for each tumor. We make this assumption for model fitting, but estimate μ_i for the purposes of model validation below, in order to strengthen the likelihood of simple alternative models.

Given a model f and parameters $\boldsymbol{p}_i, \mu_i, \sigma_i$, the conditional log-likelihood is given by

$$\begin{aligned} \log L(\boldsymbol{y}_i \mid f, \boldsymbol{p}_i, \mu_i, \sigma_i) = &- n_i \log(\sqrt{2\pi}\sigma_i) \\ &- \frac{1}{2}\sum_{j=1}^{n_i} \left(\frac{y_i(t_j) - f(\boldsymbol{p}_i, t_j) - \mu_i}{\sigma_i} \right)^2 \end{aligned} \tag{7}$$

For the purposes of model fitting, we estimated $\hat{\boldsymbol{p}}_i$ for fixed σ_i using a Markov chain Monte Carlo,[1] under the assumption that $\mu_i = 0$. We linearly interpolated our data $\boldsymbol{y_i} \mapsto \tilde{\boldsymbol{y}}_{\boldsymbol{i}}$ so that we had 5 data points per day. Per standard practice, we employ the ℓ_2 error as the target function g, for which $e^g \propto L$:

$$\begin{aligned} g(\tilde{\boldsymbol{y}}_{\boldsymbol{i}} \mid f, \hat{\boldsymbol{p}}_i, \mu_i, \sigma_i) &= -||\tilde{\boldsymbol{y}}_{\boldsymbol{i}} - \boldsymbol{f}(\hat{\boldsymbol{p}}_i)||_{\ell^2}^2 \\ &= -\sum_{j=1}^{n_i} (\tilde{y}_i(t_j) - f(\hat{\boldsymbol{p}}_i, t_j))^2 \end{aligned} \tag{8}$$

In order to favor smoother, less irregular fits, we linearly interpolated our data

[1] We use the MCMC implementation from the R package `BayesianTools`, employing the differential evolution sampler 'DEzs'.

To find $\boldsymbol{f}(\boldsymbol{p}_i)$, we need to solve systems (1, 2, 3, 4). The one-dimensional systems $2, 3$ have well-known closed-form solutions:

$$C(t) = \mu \exp\left[e^{-\alpha t} \log\left(\frac{C_0}{\mu}\right)\right] \tag{9}$$

$$C(t) = \frac{\mu C_0}{C_0 + (\mu - C_0)e^{-\alpha t}} \tag{10}$$

For our main model (1) and the two compartment model (4), we solved our equations numerically using the R package `diffeqr`, which is a convenient wrapper for the Julia suite `DifferentialEquations.jl`.

To validate our model, we compared it to each alternative choices of f for each tumor i, using the standard Bayesian Information Criterion (BIC):

$$BIC_i = N_p \log(n_i) - 2 \log \hat{L} \tag{11}$$

where N_p is the number of free parameters for our model, i.e. the length of $(\boldsymbol{p}_i, \sigma_i)$. In particular, these are $7, 4, 4, 6$ for models (1),(2),(3), and (4), respectively. Substituting (7) into (11) and using our estimate $\boldsymbol{p}_i$, we have

$$BIC_i = N_p \log(n_i) + 2n_i \log\sqrt{2\pi}\hat{\sigma}_i + \frac{1}{\hat{\sigma}_i^2}||\boldsymbol{y_i} - \boldsymbol{f}(\hat{\boldsymbol{p}}_i)||_{\ell^2}^2 \tag{12}$$

$$BIC_i = N_p \log(n_i) + 2n_i \log(\hat{\sigma}_i) + n_i(1 + \log(2\pi)) \tag{13}$$

$$\text{where } \hat{\sigma}_i^2 = \frac{||\boldsymbol{y_i} - \boldsymbol{f}(\hat{\boldsymbol{p}}_i)||_{\ell^2}^2}{n_i} \tag{14}$$

C Supplementary Tables

Table 2 Estimated Model Parameter Values. The estimated values of the (non-fixed) model parameters for each mouse tumor (from the experiment for Fig. 5E in [40]), based on tumor volume time series data.

Tumor	α	μ	ℓ	r	s_H	s_K
Scramble 1	4.60E-01	2.62E+03	1.50E-01	5.27E-02	1.50E-07	5.13E-04
Scramble 2	4.69E-01	6.91E+03	1.43E-01	1.83E-02	3.17E-06	2.74E-04
Scramble 3	4.52E-01	2.86E+03	1.45E-01	2.04E-02	3.94E-06	4.20E-05
Scramble 4	3.94E-01	3.74E+03	2.69E-02	4.79E-04	4.72E-06	1.67E-05
Scramble 5	4.80E-01	5.21E+03	7.77E-02	1.49E-02	1.01E-08	9.99E-04
Scramble 6	3.85E-01	8.49E+03	1.21E-01	1.10E-02	2.22E-08	1.89E-06
Scramble 7	3.72E-01	1.24E+03	9.75E-03	9.07E-02	5.35E-04	1.36E-08
Scramble 8	5.12E-01	4.71E+03	1.10E-01	2.26E-02	3.94E-08	9.59E-04
LSD1 KO 1	2.98E-01	1.67E+03	5.20E-02	7.06E-02	1.03E-06	2.80E-05
LSD1 KO 2	2.81E-01	8.99E+03	1.89E-02	6.80E-02	1.07E-04	1.12E-08
LSD1 KO 3	2.32E-01	2.55E+03	3.99E-02	7.95E-02	7.51E-05	4.99E-06
LSD1 KO 4	3.80E-01	6.30E+03	1.22E-01	7.92E-02	3.03E-05	9.23E-04
LSD1 KO 5	3.56E-01	4.63E+03	7.19E-02	1.73E-03	5.54E-08	1.74E-06
LSD1 KO 6	2.83E-01	8.16E+03	1.02E-03	2.77E-03	6.24E-04	2.56E-04
LSD1 KO 7	2.84E-01	5.03E+02	6.68E-02	1.56E-02	7.29E-05	3.13E-04
LSD1 MDA5 DKO 1	4.65E-01	3.39E+03	1.17E-01	2.38E-02	2.05E-07	1.71E-04
LSD1 MDA5 DKO 2	4.72E-01	3.47E+03	7.70E-02	4.00E-02	1.61E-07	9.65E-04
LSD1 MDA5 DKO 3	3.96E-01	5.18E+03	1.34E-01	1.14E-02	4.86E-08	1.32E-05
LSD1 MDA5 DKO 4	4.34E-01	3.94E+03	2.48E-02	9.29E-04	1.44E-06	8.81E-06
LSD1 MDA5 DKO 5	5.04E-01	3.34E+03	9.27E-02	2.71E-02	1.04E-08	9.64E-04
LSD1 MDA5 DKO 6	5.03E-01	7.25E+03	1.11E-01	2.76E-02	3.21E-08	9.55E-04

Table 3 Logistic Growth for Immune Deficient Tumors. To account for the possibility of immune-independent mechanisms of inhibited growth in LSD1-KO tumors, we computed the least squares estimate of logistic growth for TCRα-KO and TCRα/LSD1-DKO tumors (from Fig. 5C in [40]). We compare the means of parameters α, μ, and C_0 between the two conditions via unpaired t.test. Even pre-FDR adjustment, we find no significant difference between μ and C_0 of our samples ($t = 0.73, 1.36$, and $P = 0.476, 0.193$, respectively), and marginal evidence that the LSD1-KO condition has a *higher* immune-deficient growth rate than the control scramble ($t = -2.35$, $P = 0.038$). This latter difference vanishes after adjustment. Thus, for immunodeficient mice, we see no evidence for any anti-tumor effects of LSD1 inhibition.

Tumor	α	μ	C_0
Scramble TCRα KO 1	0.563743699	3912.194739	0.052569707
Scramble TCRα KO 2	0.480629132	4581.405315	0.137067466
Scramble TCRα KO 3	0.533601886	9990.79188	0.124822197
Scramble TCRα KO 4	0.262316687	9999.356249	9.160142923
Scramble TCRα KO 5	0.452943779	2437.152773	0.551289523
Scramble TCRα KO 6	0.349057835	5360.823555	1.827053661
Scramble TCRα KO 7	0.509650981	9987.564364	0.214161265
Scramble TCRα KO 8	0.580677922	2852.511648	0.229292158
LSD1 KO TCRα KO 1	0.334763587	9978.038937	2.40658147
LSD1 KO TCRα KO 2	0.289841785	7179.317676	7.514285629
LSD1 KO TCRα KO 3	0.339625003	3870.760716	4.572794932
LSD1 KO TCRα KO 4	0.299030515	9999.841561	2.850807521
LSD1 KO TCRα KO 5	0.36148731	9979.685307	7.152464226
LSD1 KO TCRα KO 6	0.366512912	9979.305856	0.294670011
LSD1 KO TCRα KO 7	0.293537226	7208.25365	8.984451724
LSD1 KO TCRα KO 8	0.382124921	1886.942171	1.05053347
LSD1 KO TCRα KO 9	0.526204655	2787.05914	0.088720404
LSD1 KO TCRα KO 10	0.417661279	9996.276858	1.062130233
Scramble TCRα (Avg)	0.46657774	6140.225065	1.537049863
LSD1 KO TCRα (Avg)	0.361078919	7286.548187	3.597743962

D Marginal Parameter Densities

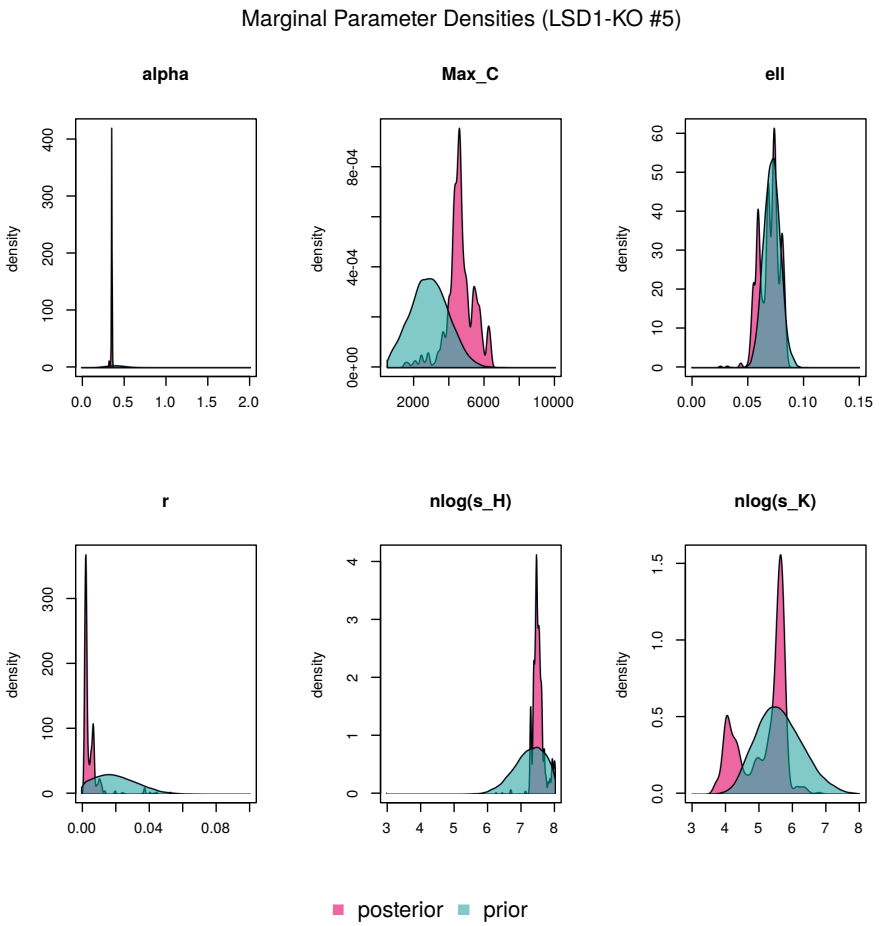

Fig. 12 Prior and Posterior Parameter Distribution for Main Model Fitting (LSD1-KO #5) Presented are the prior and posterior distribution of the parameters $\boldsymbol{p}_i$ of model 1, taken from the MCMC, where i is one of the LSD1-KO tumors. In order from left to right, the panels here correspond to $\alpha, \mu, \ell, r, \log_{10}(s_H), \log_{10}(s_K)$.

References

1. Au-Yeung, B.B., Smith, G.A., Mueller, J.L., Heyn, C.S., Jaszczak, R.G., Weiss, A., Zikherman, J.: IL-2 Modulates the TCR Signaling Threshold for CD8 but Not CD4 T Cell Proliferation on a Single-Cell Level. The Journal of Immunology **198**(6), 2445–2456 (2017). DOI 10.4049/jimmunol.1601453
2. Augert, A., Eastwood, E., Ibrahim, A.H., Wu, N., Grunblatt, E., Basom, R., Liggitt, D., Eaton, K.D., Martins, R., Poirier, J.T., Rudin, C.M., Milletti, F., Cheng, W.Y., Mack, F., MacPherson, D.: Targeting NOTCH activation in small cell lung cancer through LSD1 inhibition. Science Signaling **12**(567), eaau2922 (2019). DOI 10.1126/scisignal.aau2922. URL `http://stke.sciencemag.org/lookup/doi/10.1126/scisignal.aau2922`
3. Boulding, T., McCuaig, R.D., Tan, A., Hardy, K., Wu, F., Dunn, J., Kalimutho, M., Sutton, C.R., Forwood, J.K., Bert, A.G., Goodall, G.J., Malik, L., Yip, D., Dahlstrom,

J.E., Zafar, A., Khanna, K.K., Rao, S.: LSD1 activation promotes inducible EMT programs and modulates the tumour microenvironment in breast cancer. Scientific Reports **8**(1), 73 (2018). DOI 10.1038/s41598-017-17913-x. URL www.nature.com/scientificreports/http://www.nature.com/articles/s41598-017-17913-x

4. Chaudhary, B., Elkord, E.: Regulatory T Cells in the Tumor Microenvironment and Cancer Progression: Role and Therapeutic Targeting (2016). DOI 10.3390/vaccines4030028. URL www.mdpi.com/journal/vaccines
5. Chinen, T., Kannan, A.K., Levine, A.G., Fan, X., Klein, U., Zheng, Y., Gasteiger, G., Feng, Y., Fontenot, J.D., Rudensky, A.Y.: An essential role for the IL-2 receptor in T reg cell function. Nature Immunology **17**(11), 1322–1333 (2016). DOI 10.1038/ni.3540
6. Condamine, T., Wang, S., Diamond, M., Hall, L., Liu, H., Chadderton, A., Lu, J., He, C., Wu, L., Burn, T., Yao, W., Hollis, G., Huber, R., Ruggeri, B., Scherle, P., Koblish, H., Lee, S.H.: Abstract 4635: The LSD1 Specific Inhibitor INCB059872 enhances the activity of immune checkpoint blockade by reshaping the myeloid compartment in the syngeneic 4T1 mouse mammary tumor model (2017). DOI 10.1158/1538-7445.am2017-4635
7. Core, U.D.B.: Differential gene expression analysis in r (2019). URL https://ucdavis-bioinformatics-training.github.io/2019_March_UCSF_mRNAseq_Workshop/differential_expression/orig_DE_Analysis.html
8. De Boer, R.J., Homann, D., Perelson, A.S.: Different Dynamics of CD4 + and CD8 + T Cell Responses During and After Acute Lymphocytic Choriomeningitis Virus Infection . The Journal of Immunology (2003). DOI 10.4049/jimmunol.171.8.3928
9. De Pillis, L.G., Radunskaya, A.E., Wiseman, C.L.: A Validated Mathematical Model of Cell-Mediated Immune Response to Tumor Growth (2005). DOI 10.1158/0008-5472.CAN-05-0564. URL www.aacrjournals.org
10. Eftimie, R., Bramson, J.L., Earn, D.J.D.: Interactions Between the Immune System and Cancer: A Brief Review of Non-spatial Mathematical Models. Bulletin of Mathematical Biology **73**(1), 2–32 (2011). DOI 10.1007/s11538-010-9526-3. URL http://link.springer.com/10.1007/s11538-010-9526-3
11. Eftimie, R., Gillard, J.J., Cantrell, D.A.: Mathematical Models for Immunology: Current State of the Art and Future Research Directions. Bull Math Biol **78**, 2091–2134 (2016). DOI 10.1007/s11538-016-0214-9. URL https://search-proquest-com.proxy-um.researchport.umd.edu/docview/1830017148?accountid=14696
12. Feng, Z., Yao, Y., Zhou, C., Chen, F., Wu, F., Wei, L., Liu, W., Dong, S., Redell, M., Mo, Q., Song, Y.: Pharmacological inhibition of LSD1 for the treatment of MLL-rearranged leukemia. Journal of Hematology & Oncology **9**(1), 24 (2016). DOI 10.1186/s13045-016-0252-7. URL https://www.ncbi.nlm.nih.gov/pmc/articles/PMC4789278/pdf/13045_2016_Article_252.pdfhttp://www.jhoonline.org/content/9/1/24
13. Gadhamsetty, S., Marée, A.F., Beltman, J.B., de Boer, R.J.: A Sigmoid Functional Response Emerges When Cytotoxic T Lymphocytes Start Killing Fresh Target Cells. Biophysical Journal **112**(6), 1221–1235 (2017). DOI 10.1016/j.bpj.2017.02.008. URL https://linkinghub.elsevier.com/retrieve/pii/S0006349517301674
14. Gadhamsetty, S., Marée, A.F.M., Beltman, J.B., de Boer, R.J.: A General Functional Response of Cytotoxic T Lymphocyte-Mediated Killing of Target Cells. Biophysical Journal **106**(8), 1780–1791 (2014). DOI 10.1016/j.bpj.2014.01.048. URL http://dx.doi.org/10.1016/j.bpj.2014.01.048https://linkinghub.elsevier.com/retrieve/pii/S0006349514002185
15. Harris, W., Huang, X., Lynch, J., Spencer, G., Hitchin, J., Li, Y., Ciceri, F., Blaser, J., Greystoke, B., Jordan, A., Miller, C., Ogilvie, D., Somervaille, T.: The Histone Demethylase KDM1A Sustains the Oncogenic Potential of MLL-AF9 Leukemia Stem Cells. Cancer Cell **21**(4), 473–487 (2012). DOI 10.1016/J.CCR.2012.03.014. URL https://www.sciencedirect.com/science/article/pii/S1535610812001237?via%3Dihub
16. Hayami, S., Kelly, J.D., Cho, H.S., Yoshimatsu, M., Unoki, M., Tsunoda, T., Field, H.I., Neal, D.E., Yamaue, H., Ponder, B.A., Nakamura, Y., Hamamoto, R.: Overexpression of LSD1 contributes to human carcinogenesis through chromatin regulation in various cancers. International Journal of Cancer **128**(3), 574–586 (2011). DOI 10.1002/ijc.25349. URL http://doi.wiley.com/10.1002/ijc.25349
17. Juneja, V.R., McGuire, K.A., Manguso, R.T., LaFleur, M.W., Collins, N., Haining, W.N., Freeman, G.J., Sharpe, A.H.: PD-L1 on tumor cells is sufficient for immune evasion in immunogenic tumors and inhibits CD8 T cell cytotoxicity. The

Journal of Experimental Medicine **214**(4), 895–904 (2017). DOI 10.1084/jem.20160801. URL https://doi.org/10.1084/jem.20160801http://www.jem.org/lookup/doi/10.1084/jem.20160801

18. Kaartinen, T., Luostarinen, A., Maliniemi, P., Keto, J., Arvas, M., Belt, H., Koponen, J., Loskog, A., Mustjoki, S., Porkka, K., Ylä-Herttuala, S., Korhonen, M.: Low interleukin-2 concentration favors generation of early memory T cells over effector phenotypes during chimeric antigen receptor T-cell expansion. Cytotherapy **19**(6), 689–702 (2017). DOI 10.1016/j.jcyt.2017.03.067
19. Kalia, V., Sarkar, S.: Regulation of Effector and Memory CD8 T Cell Differentiation by IL-2-A Balancing Act (2018). DOI 10.3389/fimmu.2018.02987
20. Kashyap, V., Ahmad, S., Nilsson, E.M., Helczynski, L., ead Kenna, S., Liao Persson, J., Gudas, L.J., Mongan, N.P.: The lysine specific demethylase-1 (LSD1/KDM1A) regulates VEGF-A expression in prostate cancer (2013). DOI 10.1016/j.molonc.2013.01.003. URL http://dx.doi.org/10.1016/j.molonc.2013.01.003
21. Kavrochorianou, N., Markogiannaki, M., Haralambous, S.: IFN-β differentially regulates the function of T cell subsets in MS and EAE. Cytokine & Growth Factor Reviews **30**, 47–54 (2016). DOI 10.1016/j.cytogfr.2016.03.013. URL http://www.ncbi.nlm.nih.gov/pubmed/27033173https://linkinghub.elsevier.com/retrieve/pii/S1359610116300375
22. Kim, P.S., Lee, P.P., Levy, D.: A Theory of Immunodominance and Adaptive Regulation. Bulletin of Mathematical Biology **73**(7), 1645–1665 (2011). DOI 10.1007/s11538-010-9585-5. URL https://www.ncbi.nlm.nih.gov/pmc/articles/PMC3865720/pdf/nihms529178.pdfhttp://link.springer.com/10.1007/s11538-009-9463-1http://link.springer.com/10.1007/s11538-010-9585-5
23. Kim, P.S., Lee, P.P., Levy, D.: Basic Principles in Modeling Adaptive Regulation and Immunodominance. In: Mathematical Biosciences, vol. 257, pp. 33–57 (2013). DOI 10.1007/978-1-4614-4178-6{_}2. URL http://link.springer.com/10.1007/978-1-4614-4178-6_2
24. Kleppe, M., Shank, K., Efthymia, P., Riehnhoff, H., Levine, R.L.: Lysine-Specific Histone Demethylase, LSD1, (KDM1A) As a Novel Therapeutic Target in Myeloproliferative Neoplasms. Blood **126**(23) (2015). URL http://www.bloodjournal.org/content/126/23/601?sso-checked=true
25. Kuang, Y., Nagy, J.D., Eikenberry, S.E.: Introduction to Mathematical Oncology. Chapman and Hall/CRC (2018). DOI 10.1201/9781315365404. URL https://www.taylorfrancis.com/books/9781315361987
26. Lechner, M.G., Karimi, S.S., Barry-Holson, K., Angell, T.E., Murphy, K.A., Church, C.H., Ohlfest, J.R., Hu, P., Epstein, A.L.: Immunogenicity of murine solid tumor models as a defining feature of in vivo behavior and response to immunotherapy DOI 10.1097/01.cji.0000436722.46675.4a. URL https://www.ncbi.nlm.nih.gov/pmc/articles/PMC3910494/pdf/nihms542249.pdf
27. Lee, W., Lee, G.R.: Transcriptional regulation and development of regulatory T cells (2018). DOI 10.1038/emm.2017.313
28. Li, J.L., Sainson, R.C., Shi, W., Leek, R., Harrington, L.S., Preusser, M., Biswas, S., Turley, H., Heikamp, E., Hainfellner, J.A., Harris, A.L.: Delta-like 4 Notch Ligand Regulates Tumor Angiogenesis, Improves Tumor Vascular Function, and Promotes Tumor Growth In vivo. Cancer Research **67**(23), 11244–11253 (2007). DOI 10.1158/0008-5472.CAN-07-0969. URL http://cancerres.aacrjournals.org/lookup/doi/10.1158/0008-5472.CAN-07-0969
29. Lim, S., Janzer, A., Becker, A., Zimmer, A., Schüle, R., Buettner, R., Kirfel, J.: Lysine-specific demethylase 1 (LSD1) is highly expressed in ER-negative breast cancers and a biomarker predicting aggressive biology. Carcinogenesis **31**(3), 512–520 (2010). DOI 10.1093/carcin/bgp324. URL http://www.ncbi.nlm.nih.gov/pubmed/20042638https://academic.oup.com/carcin/article-lookup/doi/10.1093/carcin/bgp324
30. McKarns, S.C., Schwartz, R.H.: Distinct Effects of TGF-β1 on CD4 + and CD8 + T Cell Survival, Division, and IL-2 Production: A Role for T Cell Intrinsic Smad3. The Journal of Immunology **174**(4), 2071–2083 (2005). DOI 10.4049/jimmunol.174.4.2071. URL http://www.jimmunol.org/lookup/doi/10.4049/jimmunol.174.4.2071

31. McNally, A., Hill, G.R., Sparwasser, T., Thomas, R., Steptoe, R.J.: CD4+CD25+ regulatory T cells control CD8+ T-cell effector differentiation by modulating IL-2 homeostasis. Proceedings of the National Academy of Sciences of the United States of America **108**(18), 7529–7534 (2011). DOI 10.1073/pnas.1103782108
32. Niebel, D., Kirfel, J., Janzen, V., Höller, T., Majores, M., Gütgemann, I.: Lysine-specific demethylase 1 (LSD1) in hematopoietic and lymphoid neoplasms. Blood **124**(1), 151–2 (2014). DOI 10.1182/blood-2014-04-569525. URL http://www.ncbi.nlm.nih.gov/pubmed/24993879
33. Oh, S.A., Li, M.O.: TGF-β: guardian of T cell function. Journal of immunology (Baltimore, Md. : 1950) **191**(8), 3973–9 (2013). DOI 10.4049/jimmunol.1301843. URL http://www.ncbi.nlm.nih.gov/pubmed/24098055http://www.pubmedcentral.nih.gov/articlerender.fcgi?artid=PMC3856438
34. Potez, M., Trappetti, V., Bouchet, A., Fernandez-Palomo, C., Güç, E., Kilarski, W.W., Hlushchuk, R., Laissue, J., Djonov, V.: Characterization of a B16-F10 melanoma model locally implanted into the ear pinnae of C57BL/6 mice. PLoS ONE (2018). DOI 10.1371/journal.pone.0206693
35. Qin, Y., Vasilatos, S.N., Chen, L., Wu, H., Cao, Z., Fu, Y., Huang, M., Vlad, A.M., Lu, B., Oesterreich, S., Davidson, N.E., Huang, Y.: Inhibition of histone lysine-specific demethylase 1 elicits breast tumor immunity and enhances antitumor efficacy of immune checkpoint blockade. Oncogene p. 1 (2018). DOI 10.1038/s41388-018-0451-5. URL http://www.nature.com/articles/s41388-018-0451-5
36. Sakamoto, A., Hino, S., Nagaoka, K., Anan, K., Takase, R., Matsumori, H., Ojima, H., Kanai, Y., Arita, K., Nakao, M.: Lysine Demethylase LSD1 Coordinates Glycolytic and Mitochondrial Metabolism in Hepatocellular Carcinoma Cells. Cancer Research **75**(7), 1445–1456 (2015). DOI 10.1158/0008-5472.CAN-14-1560. URL http://www.ncbi.nlm.nih.gov/pubmed/25649769http://cancerres.aacrjournals.org/lookup/doi/10.1158/0008-5472.CAN-14-1560
37. Schenk, T., Chen, W.C., Göllner, S., Howell, L., Jin, L., Hebestreit, K., Klein, H.U., Popescu, A.C., Burnett, A., Mills, K., Casero, R.A., Marton, L., Woster, P., Minden, M.D., Dugas, M., Wang, J.C.Y., Dick, J.E., Müller-Tidow, C., Petrie, K., Zelent, A., Zelent, A.: Inhibition of the LSD1 (KDM1A) demethylase reactivates the all-trans-retinoic acid differentiation pathway in acute myeloid leukemia. Nature medicine **18**(4), 605–11 (2012). DOI 10.1038/nm.2661. URL http://www.ncbi.nlm.nih.gov/pubmed/22406747http://www.pubmedcentral.nih.gov/articlerender.fcgi?artid=PMC3539284
38. Segarra, M., Williams, C.K., De La, M., Sierra, L., Bernardo, M., Mccormick, P.J., Maric, D., Regino, C., Choyke, P., Tosato, G.: Dll4 activation of Notch signaling reduces tumor vascularity and inhibits tumor growth DOI 10.1182/blood-2007-11-126045. URL www.bloodjournal.org
39. Serce, N., Gnatzy, A., Steiner, S., Lorenzen, H., Kirfel, J., Buettner, R.: Elevated expression of LSD1 (Lysine-specific demethylase 1) during tumour progression from pre-invasive to invasive ductal carcinoma of the breast. BMC clinical pathology **12**, 13 (2012). DOI 10.1186/1472-6890-12-13. URL http://www.ncbi.nlm.nih.gov/pubmed/22920283http://www.pubmedcentral.nih.gov/articlerender.fcgi?artid=PMC3511290
40. Sheng, W., LaFleur, M.W., Nguyen, T.H., Chen, S., Chakravarthy, A., Conway, J.R., Li, Y., Chen, H., Yang, H., Hsu, P.H., Van Allen, E.M., Freeman, G.J., De Carvalho, D.D., He, H.H., Sharpe, A.H., Shi, Y.: LSD1 Ablation Stimulates Anti-tumor Immunity and Enables Checkpoint Blockade. Cell **174**(3), 549–563 (2018). DOI 10.1016/j.cell.2018.05.052. URL http://www.ncbi.nlm.nih.gov/pubmed/29937226http://www.pubmedcentral.nih.gov/articlerender.fcgi?artid=PMC6063761
41. Siekmann, A.F., Lawson, N.D., Siekmann, A.F., Lawson, N.D.: Extra View Notch Signalling and the Regulation of Angiogenesis Addendum to: Notch Signalling Limits Angiogenic Cell Behavior in Developing Zebrafish Arteries. Tech. Rep. 2 (2007). URL http://www.landesbioscience.com/journals/celladhesion/article/4488
42. Song, M., Chen, X., Wang, L., Zhang, Y.: Future of anti-PD-1/PD-L1 applications: Combinations with other therapeutic regimens. Chinese journal of cancer research = Chung-kuo yen cheng yen chiu **30**(2), 157–172 (2018). DOI 10.21147/j.issn.

1000-9604.2018.02.01. URL http://www.ncbi.nlm.nih.gov/pubmed/29861603http://www.pubmedcentral.nih.gov/articlerender.fcgi?artid=PMC5953954

43. Tammela, T., Zarkada, G., Wallgard, E., Murtomäki, A., Suchting, S., Wirzenius, M., Waltari, M., Hellström, M., Schomber, T., Peltonen, R., Freitas, C., Duarte, A., Isoniemi, H., Laakkonen, P., Christofori, G., Ylä-Herttuala, S., Shibuya, M., Pytowski, B., Eichmann, A., Betsholtz, C., Alitalo, K.: Blocking VEGFR-3 suppresses angiogenic sprouting and vascular network formation. Nature **454**(7204), 656–660 (2008). DOI 10.1038/nature07083. URL http://www.nature.com/articles/nature07083
44. Wodarz, D., Komarova, N.L.: Dynamics of Cancer. WORLD SCIENTIFIC (2014). DOI 10.1142/8973. URL https://www.worldscientific.com/worldscibooks/10.1142/8973
45. Woo, S.R., Fuertes, M.B., Corrales, L., Spranger, S., Furdyna, M.J., Leung, M.Y.K., Duggan, R., Wang, Y., Barber, G.N., Fitzgerald, K.A., Alegre, M.L., Gajewski, T.F.: STING-Dependent Cytosolic DNA Sensing Mediates Innate Immune Recognition of Immunogenic Tumors. Immunity **41**(5), 830–842 (2014). DOI 10.1016/j.immuni.2014.10.017. URL http://dx.doi.org/10.1016/j.immuni.2014.10.017https://linkinghub.elsevier.com/retrieve/pii/S1074761314003938
46. Wyatt, A.: Mathematical Models of Acute and Chronic Immunology. Ph.D. thesis, University of Maryland (2019)
47. Yan, Y., Kumar, A.B., Finnes, H., Markovic, S.N., Park, S., Dronca, R.S., Dong, H.: Combining Immune Checkpoint Inhibitors With Conventional Cancer Therapy. Frontiers in immunology **9**, 1739 (2018). DOI 10.3389/fimmu.2018.01739. URL http://www.ncbi.nlm.nih.gov/pubmed/30100909http://www.pubmedcentral.nih.gov/articlerender.fcgi?artid=PMC6072836
48. Yang, G.J., Lei, P.M., Wong, S.Y., Ma, D.L., Leung, C.H.: Pharmacological Inhibition of LSD1 for Cancer Treatment. Molecules (Basel, Switzerland) **23**(12) (2018). DOI 10.3390/molecules23123194. URL http://www.ncbi.nlm.nih.gov/pubmed/30518104http://www.pubmedcentral.nih.gov/articlerender.fcgi?artid=PMC6320820
49. Ye, C., Brand, D., Zheng, S.G.: Targeting IL-2: an unexpected effect in treating immunological diseases (2018). DOI 10.1038/s41392-017-0002-5
50. Zafranskaya, M., Oschmann, P., Engel, R., Weishaupt, A., van Noort, J.M., Jomaa, H., Eberl, M.: Interferon-beta therapy reduces CD4+ and CD8+ T-cell reactivity in multiple sclerosis. Immunology **121**(1), 29–39 (2007). DOI 10.1111/j.1365-2567.2006.02518.x. URL http://www.ncbi.nlm.nih.gov/pubmed/17239199http://www.pubmedcentral.nih.gov/articlerender.fcgi?artid=PMC2265917
51. Zheng, H., Jin, B., Henrickson, S.E., Perelson, A.S., von Andrian, U.H., Chakraborty, A.K.: How Antigen Quantity and Quality Determine T-Cell Decisions in Lymphoid Tissue. Molecular and Cellular Biology **28**(12), 4040–4051 (2008). DOI 10.1128/MCB.00136-08. URL https://www.ncbi.nlm.nih.gov/pmc/articles/PMC2423119/pdf/0136-08.pdfhttp://mcb.asm.org/cgi/doi/10.1128/MCB.00136-08